ORIGINAL ARTICLE

Homotopy study of magnetohydrodynamic mixed convection nanofluid multiple slip flow and heat transfer from a vertical cylinder with entropy generation

Nisha Shukla[a], Puneet Rana[a,*], O. Anwar Bég[b], Bani Singh[a], A. Kadir[c]

[a]*Department of Mathematics, Jaypee Institute of Information Technology, A-10, Sector-62, Noida 201307, Uttar Pradesh, India*
[b]*Fluid Mechanics, Propulsion and Nanosystems, Aeronautical and Mechanical Engineering, School of Computing, Science & Engineering, University of Salford, Newton Building, M54WT, UK*
[c]*Materials and Corrosion, Petroleum and Gas Engineering, School of Computing, Science & Engineering, University of Salford, Newton Building, M54WT, UK*

Abstract Stimulated by thermal optimization in magnetic materials process engineering, the present investigation investigates theoretically the entropy generation in mixed convection magnetohydrodynamic (MHD) flow of an electrically-conducting nanofluid from a vertical cylinder. The mathematical model includes the effects of viscous dissipation, second order velocity slip and thermal slip, has been considered. The cylindrical partial differential form of the two-component non-homogenous nanofluid model has been transformed into a system of coupled ordinary differential equations by applying similarity transformations. The effects of governing parameters with no-flux nanoparticle concentration have been examined on important quantities of interest. Furthermore, the dimensionless form of the entropy generation number has also been evaluated using homotopy analysis method (HAM). The present analytical results achieve good correlation with numerical results (shooting method). Entropy is found to be an increasing function of second order velocity slip, magnetic field and curvature parameter. Temperature is elevated with increasing curvature parameter and magnetic parameter whereas it is reduced with mixed convection parameter. The flow is accelerated

*Corresponding author.

E-mail addresses: puneetranaiitr@gmail.com, puneet.rana@jiit.ac.in (Puneet Rana).

with curvature parameter but decelerated with magnetic parameter. Heat transfer rate (Nusselt number) is enhanced with greater mixed convection parameter, curvature parameter and first order velocity slip parameter but reduced with increasing second order velocity slip parameter. Entropy generation is also increased with magnetic parameter, second order slip velocity parameter, curvature parameter, thermophoresis parameter, buoyancy parameter and Reynolds number whereas it is suppressed with first order velocity slip parameter, Brownian motion parameter and thermal slip parameter.

1. Introduction

External boundary layer flows of nanofluids [1] find substantial applications in numerous industries and engineering fields including materials synthesis, biomedicine, nuclear reactor cooling, electronics, propellants, combustion and automotive radiator systems [2] etc. The suspension of nanoparticles in a base fluid is referred as a nanofluid [3,4]. The transport behavior in nanofluids can be described by two mathematical models i.e. homogeneous or non-homogeneous models. In case of non-homogenous modeling, Buongiorno [5] identified that Brownian diffusion and thermophoresis contribute significantly to thermal enhancement in nanofluids. Mathematical and experimental modelling of convective heat transfer in nanofluids has received significant attention in applied mathematics and engineering sciences, largely due to emerging applications in materials processing. Sheikholeslami and Rokni [6] have analyzed the impact of induced magnetic field on nanofluid flow through two vertical porous plates using two phase model. Rana et al. [7] have evaluated dual solutions of Al_2O_3-water nanofluid flow induced by horizontal cylinder using modified Buongiorno's model. The study of magnetic nanofluid flow has numerous applications in industries. Sheikholeslami and Zeeshan [8] have analyzed the magnetic field effect on water based nanofluid flow. In this series, a number of authors have examined different types of study of fluid flow and heat transfer utilizing nanoparticles [9–13].

Earlier studies include Kuznetsov et al. [14] and Aziz et al. [15] who examined the natural convective boundary-layer flow of a nanofluid from a vertical plate using Buongiorno's model. Sheikholeslami [16–18] and Sheikholeslami and Rokni [19] have examined the natural convection of MHD nanofluid on different geometries explaining the influence of various physical parameters. Mahgoub [20] studied the forced convection heat transfer over a horizontal flat plate experimentally, observing that larger particles with high thermal conductivity have a high heat transfer coefficient. Hatami et al. [21] derived analytical solutions for forced convection boundary layer flow of hydromagnetic flow of alumina-water nanofluid along a stretching sheet using the homotopy analysis method. Sheikholeslami [22,23] has applied Lattice Boltzmann method to investigate forced convection on magnetohydrodynamic (MHD) nanofluid flow. The study of mixed convection heat transfer is more generalized since the value of mixed convection parameter (e.g. Richardson number) can be modulated to achieve natural or forced convection heat transfer or both. Nazar et al. [24] studied the mixed convection nanofluid boundary layer flow from an isothermal horizontal circular cylinder. Rana et al. [25] have presented finite element solutions for the mixed convection flow of alumina-water nanofluid over an inclined hollow cylinder with wall conduction effects. Recently, Trîmbitas et al. [26] derived dual solutions for the mixed convection boundary layer nanofluid flow from a vertical semi-infinite plate. They also investigated the stability of solutions to identify the physically realistic solution.

The no-slip condition is a classical boundary condition in fluid dynamics which is imposed at a solid boundary. Here the fluid is prescribed to have zero velocity relative to the boundary. However there are so many situations in which this condition does not provide appropriate results, especially for the flow of nanofluids and non-Newtonian fluids. To study such flows more accurately, slip conditions are required. Yoshimura et al. [27] have investigated the partial slip condition and assumed that the first order derivatives of velocity and stress have some non-zero finite values at the boundary. Anderson [28] has obtained a solution of Navier-Stokes equations for the MHD slip flow over a stretching surface. Rana et al. [29] have analyzed the slip effects on MHD nanofluid stagnation point flow over a nonlinear stretching sheet. Zheng et al. [30] studied hydrodynamic and thermal slip effects in radiative convection nanofluid flow over a stretching sheet embedded in a permeable regime. Dhanai et al. [31] investigated the critical values of mixed convection parameter for the existence of dual solutions in MHD mixed convection nanofluid flow over an inclined cylinder with first order velocity slip and thermal slip effects using Buongiorno's model. Dhanai et al. [32] have applied Lie group analysis to investigate

Nomenclature

A	a constant in velocity slip model (unit: m)
B	a constant in velocity slip model (unit: m^2)
B_0	magnetic field strength (unit: $A \cdot m^{-1}$)
C	nanoparticle volume fraction
C_∞	ambient volume fraction
D	diffusion (unit: $m^2 \cdot s^{-1}$)
D_B	Brownian diffusion coefficient (unit: $m^2 \cdot s^{-1}$)
D_T	thermophoretic diffusion coefficient (unit: $m^2 \cdot s^{-1}$)
Ec	Eckert number
Nb	Brownian motion parameter
Nt	thermophoresis parameter
Nr	buoyancy ratio
Pr	Prandtl number
q_w	wall heat flux (unit: $W \cdot m^{-2}$)
r	radial coordinate (unit: m)
R	gas constant (unit: $J \cdot mol^{-1} \cdot K^{-1}$)
Ri	Richardson number
Sc	Schmidt number
f	dimensionless stream function
g	gravitational acceleration (unit: $m \cdot s^{-2}$)
Gr	Grashof number
k	thermal conductivity (unit: $W \cdot m^{-1} \cdot K^{-1}$)
K_n	Knudsen number
M	dimensionless magnetic field
N	thermal slip factor
T	nanofluid temperature (unit: K)
T_w	nanofluid temperature at surface (unit: K)
u	velocity components along radial axis direction (unit: $m \cdot s^{-1}$)
w	velocity components along z-axis direction (unit: $m \cdot s^{-1}$)
W_w	velocity of cylinder (unit: $m \cdot s^{-1}$)
u_w	mass transfer velocity (unit: $m \cdot s^{-1}$)
z	cylindrical polar coordinates (unit: m)

Greek letters

η	similarity variable
μ	dynamic viscosity (unit: $N \cdot s \cdot m^{-2}$)
ϕ	dimensionless nanoparticle concentration
θ	dimensionless temperature
υ	kinematic viscosity (unit: $m^2 \cdot s^{-1}$)
α	thermal diffusivity (unit: $m^2 \cdot s^{-1}$)
λ	molecular mean free path (unit: m)
γ	curvature parameter
$\lambda_1 \ \lambda_2$	first and second order velocity slip parameters
δ	thermal slip parameter
$(\rho c)_f$	heat capacity of basefluid (unit: $J \cdot K^{-1} \cdot m^{-3}$)
$(\rho c)_p$	effective heat capacity of nanoparticle material (unit: $J \cdot K^{-1} \cdot m^{-3}$)
χ	diffusive constant parameter
τ_w	shear stress at surface (unit: $N \cdot m^{-2}$)
β	thermal expansion coefficient (unit: K^{-1})
Ω	dimensionless temperature
ψ	stream function (unit: $m^2 \cdot s^{-1}$)
ρ	density (unit: $kg \cdot m^{-3}$)
σ	electric conductivity of basefluid (unit: $S \cdot m^{-1}$)
α_m	momentum accommodation coefficient

Subscripts

f	fluid
p	nanoparticle
∞	ambient condition
w	condition on surface

the slip effects on MHD bioconvection flow over an inclined sheet. Recently, Rana et al. [33] have investigated dual solutions of radiative nanofluid flow with slip effects.

Introduced for rarefied gas flows, the dimensionless Knudsen number represents the ratio of the molecular mean free path length to the representative length scale. For large values of Knudsen number, the first order slip model provides erroneous results and therefore, the second order slip model has been investigated by a number of researchers. Wu [34] considered the second order velocity slip model for gases (rarefied fluids). This model is equivalent to the Fukui-Kaneko model based on the numerical simulation of the linearized Boltzmann equations. Fang et al. [35] have derived dual solutions for the viscous flow over a shrinking sheet using the second order slip flow model. Zhu et al. [36] have investigated the magnetic convection flow of nanofluid from a permeable stretching sheet with second order velocity slip using the homotopy analysis method. Sharma et al. [37] have studied numerically the second order slip flow and heat transfer of Cu-water based nanofluid from a stretching sheet by applying the finite element method. Mabood et al. [38] have simulated second order slip and

viscous dissipation effects in magnetohydrodynamic flow of nanofluid from a stretching sheet.

Although the above studies have addressed a wide range of problems related to first and second order velocity slip effects over stretching/shrinking sheets, they have never-
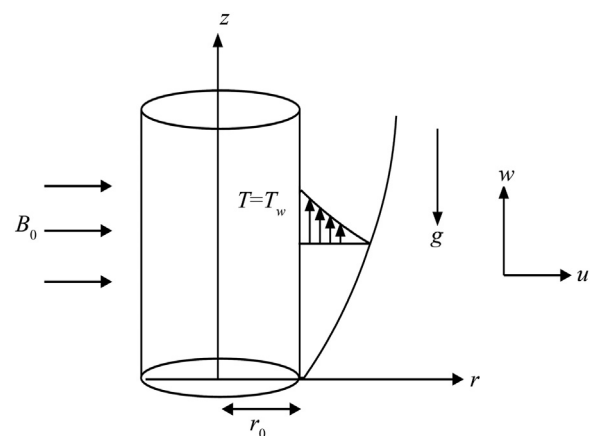

Figure 1 Geometry of problem.

theless been restricted from the thermodynamic point of view i.e. they have only considered the first law of thermodynamics (energy conservation). In thermo-dynamic systems, energy is destroyed due to irreversibility which includes magnetic forces, viscous dissipation, thermal gradient, diffusion and chemical reactions. This results in entropy generation in these thermal systems. The general equation of the entropy generation for forced convective heat transfer from a plate and circular cylinder has been derived by Bejan [39,40]. Aiboud et al. [41] have studied the effects of magnetic field and Reynolds number on the entropy generation rate for viscoelastic flow along a stretching sheet. Abolbashari et al. [42] have analysed entropy generation in Casson (viscoplastic) nanofluid flow over a stretching sheet using an optimal homotopy analysis method. The same analysis has been presented by Noghre-habadi et al. [43] for the nanofluid flow over a stretching sheet with the effect of first order velocity slip at the boundary.

Liao [44,45] has proposed a powerful analytical technique, termed the homotopy analysis method (HAM), which provides power series solutions for nonlinear differential equations. This technique does not contain any small or large parameters, as is customary with conventional perturbation techniques [46]. Furthermore, HAM also provides an easier approach to ensure convergence of the series of solution. A number of researchers [47–50] have successfully applied this method in a variety of multi-physical problems. The major purpose of present article is to investigate the effects of thermal and second order velocity slip on a MHD mixed convection nanofluid flow over a vertical cylinder with entropy generation analysis using homotopy analysis method. This scenario has not yet received the attention of researchers in the technical literature and is relevant to more accurate magnetic nanomaterials processing systems and thermodynamic optimization of such systems.

2. Magnetic dissipative nanofluid flow model

Consider the two-dimensional, steady, boundary layer flow of incompressible nanofluid over an infinite vertical cylinder which is stretched with velocity $W_w = W_0 z$. A cylindrical coordinate system (r, z) is employed. The geometry of the problem is visualized in Figure 1. The nanofluid is electrically-conducting and is subjected to a constant magnetic field B_0 applied in the radial direction. It is assumed that the temperature of the surface of cylinder is T_w and the ambient temperature is T_∞ $(T_\infty < T_w)$. Due to difference between the temperature of surface of cylinder and the surrounding nanofluid, a thermal buoyancy force is generated force is generated in the upward direction. At the cylinder surface the concentration is controlled by the condition $D_B \frac{\partial C}{\partial r} + \frac{D_T}{T_\infty} \frac{\partial T}{\partial r} = 0$, whereas C_∞ represents the ambient concentration. Concentration differences between

the cylinder surface and ambient nanofluid also generate a species (solutal) buoyancy force. The effects of pressure gradient and external forces are neglected. Under these assumptions, the governing equations for nanofluid boundary layer flow along the cylinder can be written as (see [31,51]):

$$\frac{1}{r}\frac{\partial}{\partial r}(ru) + \frac{\partial w}{\partial z} = 0 \tag{1}$$

$$u\frac{\partial w}{\partial r} + w\frac{\partial w}{\partial z} = \frac{\nu}{r}\frac{\partial}{\partial r}\left(r\frac{\partial w}{\partial r}\right) - \frac{\sigma B_0^2}{\rho}w$$
$$+ \left[-\frac{(\rho_p - \rho)(C - C_\infty)}{\rho} + (1 - C_\infty)(T - T_\infty)\beta\right]g \tag{2}$$

$$(\rho c)_f \left(u\frac{\partial T}{\partial r} + w\frac{\partial T}{\partial z}\right) = \frac{k}{r}\frac{\partial}{\partial r}\left(r\frac{\partial T}{\partial r}\right)$$
$$+ (\rho c)_p \left[D_B \frac{\partial C}{\partial r}\frac{\partial T}{\partial r} + \frac{D_T}{T_\infty}\left(\frac{\partial T}{\partial r}\right)^2\right] + \mu\left(\frac{\partial w}{\partial r}\right)^2 \tag{3}$$

$$u\frac{\partial C}{\partial r} + w\frac{\partial C}{\partial r} = \frac{D_B}{r}\frac{\partial}{\partial r}\left(r\frac{\partial C}{\partial r}\right) + \frac{D_T}{T_\infty}\frac{1}{r}\frac{\partial}{\partial r}\left(r\frac{\partial T}{\partial r}\right) \tag{4}$$

Here u and w are components of velocity considered along the r- and z-axis respectively, υ is kinematic viscosity, ρ_p and ρ are densities of nanoparticles and fluid respectively, β is volumetric thermal expansion coefficient of nanofluid, g is gravitational acceleration. σ represents the electrical conductivity of nanofluid, k is the thermal conductivity, $(\rho c)_f$ and $(\rho c)_p$ are the heat capacities of base fluid and nanoparticles respectively, T is temperature of nanofluid, C is concentration of nanoparticles, μ indicates the dynamic viscosity and D_B and D_T are Brownian and thermophoresis diffusion coefficients. The boundary conditions for velocity, temperature and nano-particles concentration are defined as [31,34]

at $r = r_0\ w(zr) = W_w + W_s\ u_w = u_w(z)$
$$T = T_w + N\frac{\partial T}{\partial r}\ D_B\frac{\partial C}{\partial r} + \frac{D_T}{T_\infty}\frac{\partial T}{\partial r} = 0$$
as $r \to \infty\ w(zr) = 0\ T = T_\infty\ C = C_\infty \tag{5}$

where N is thermal slip factor. The velocity slip W_s is defined as [35,36]:

$$W_s = \frac{2}{3}\left(\frac{3 - \alpha_m l^3}{\alpha_m} - \frac{3}{2}\frac{1 - l^2}{K_n}\right)\lambda\frac{\partial w}{\partial r} - \frac{1}{4}\left(l^4 + \frac{2}{K_n^2}\left(1 - l^2\right)\right)$$

$$\lambda^2\frac{\partial^2 w}{\partial r^2} = A\frac{\partial w}{\partial r} + B\frac{\partial^2 w}{\partial r^2} \tag{6}$$

where $l = \min\left(\frac{1}{K_n}, 1\right)$ K_n is Knudsen number, $0 \le \alpha_m \le 1$ where α_m is momentum accommodation coefficient and λ is mean free path. The value of l is lies between 0 and 1.

To convert Eqs. (1)–(4) and boundary conditions (5) into non-dimensional form, we have applied the following

similarity transformations [31]:

$$\eta = \frac{r^2 - r_0^2}{2r_0}\sqrt{\frac{W_0}{v}} \quad \psi = \sqrt{W_0 v z r_0}\, f(\eta) \quad w = W_0 z f'(\eta),$$

$$u = -\frac{r_0}{r}\sqrt{W_0 v}\, f(\eta), \quad \theta = \frac{T - T_\infty}{T_w - T_\infty}, \quad \phi = \frac{C - C_\infty}{C_\infty} \qquad (7)$$

where η is similarity variable (transformed radial coordinate), ψ is stream function defined as $u = -\frac{1}{r}\frac{\partial \psi}{\partial r}$ and $w = \frac{1}{r}\frac{\partial \psi}{\partial z}$ which satisfies Eq. (1) and prime denotes the differentiation with respect to η. Applying similarity transformations (7) on Eqs. (2)–(5) yields the following coupled system of ordinary differential equations for momentum, energy and species (nano-particle) conservation:

$$(1 + 2\eta\gamma)f''' + 2\gamma f'' - f'^2 + ff'' - M^2 f'$$
$$+ Ri(\theta - Nr\phi) = 0, \qquad (8)$$

$$\frac{1}{Pr}\left[(1 + 2\eta\gamma)\left(\theta'' + Nb\theta'\phi' + Nt\theta'^2\right) + 2\gamma\theta'\right]$$
$$+ (1 + 2\eta\gamma)Ec f''^2 + f\theta' = 0, \qquad (9)$$

$$(1 + 2\eta\gamma)\phi'' + 2\gamma\phi' + 2\left(\frac{Nt}{Nb}\right)\gamma\theta' + (1 + 2\eta\gamma)\frac{Nt}{Nb}\theta''$$
$$+ Sc f\phi' = 0, \qquad (10)$$

The boundary conditions are transformed to

at $\eta = 0$, $f(0) = 0$, $f'(0) = 1 + \lambda_1 f''(0) + \lambda_2 f'''(0)$,
$\theta = 1 + \delta\theta'(0)$, $Nb\phi'(0) + Nt\theta'(0) = 0$,
and as $\eta \to \infty$, $f'(\eta) = 0$, $\theta(\eta) = 0$, $\phi(\eta) = 0$ (11)

where $\gamma = \sqrt{\frac{v}{r_0^2 W_0}}$ is cylinder curvature parameter, $M = \sqrt{\frac{\sigma B_0^2}{W_0 \rho}}$ is magnetic body force parameter, $Gr = \frac{\beta g(T_w - T_\infty)z^3}{v^2}$ is thermal local Grashof number, $Ri = \frac{g\beta(T_w - T_\infty)z}{W_0^2}$ is local Richardson number, $Re = \frac{W_0 z^2}{v}$ is local Reynolds number, $Nr = \frac{(\rho_p - \rho)C_\infty}{\beta\rho(1 - C_\infty)(T_w - T_\infty)}$ is buoyancy ratio parameter, $Pr = \frac{v}{\alpha}$ is Prandtl number, $Ec = \frac{W_w^2}{c_f(T_w - T_\infty)}$ is Eckert number, $Nb = \frac{(\rho c)_p}{(\rho c)_f \alpha}D_B C_\infty$ is Brownian motion parameter, $Nt = \frac{(\rho c)_p}{(\rho c)_f \alpha}\frac{D_T}{T_\infty}(T_w - T_\infty)$ is thermophoresis parameter, $Sc = \frac{v}{D_B}$ is Schmidt number, $\lambda_1 = \left(A + \frac{B}{r_0}\right)\sqrt{\frac{W_0}{v}}$ is first order velocity (hydrodynamic) slip parameter, $\lambda_2 = B\frac{W_0}{v}$ is second order velocity (hydrodynamic) slip parameter and $\delta = N\sqrt{\frac{W_0}{v}}$ is thermal slip (jump) parameter. In this study, skin friction coefficient C_f and local Nusselt number are the quantities of practical interest which are expressed as:

$$C_f = \frac{\tau_w}{\rho w_w^2}, \quad Nu_z = \frac{z q_w}{k(T_w - T_\infty)} \qquad (12)$$

where k is thermal conductivity, τ_w is shear stress at wall

and q_w is the wall heat flux. The shear stress τ_w and heat flux q_w are defined as

$$\tau_w = \mu\left(\frac{\partial w}{\partial r}\right)_{r = r_0}, \quad q_w = -k\frac{\partial T}{\partial r}\bigg|_{r = r_0} - h_p \rho_p\left(D_B\frac{\partial C}{\partial r} + \frac{D_T}{T}\frac{\partial T}{\partial r}\right)_{r = r_0} \qquad (13)$$

Using Eqs. (7) and (13) in Eq. (12), we obtain

$$Re^{1/2} C_f = f''(0), \quad Re^{-1/2} Nu_z = -\theta'(0). \qquad (14)$$

3. Second law (entropy generation analysis)

As mentioned in Refs. [39,40] the local volumetric rate of entropy generation in the presence of a magnetic field is defined as:

$$S_{gen} = \underbrace{\frac{k}{T_\infty^2}\left(\frac{\partial T}{\partial r}\right)^2}_{\text{EG due to heat transfer}} + \underbrace{\frac{\mu}{T_\infty}\left(\frac{\partial w}{\partial r}\right)^2}_{\text{EG due to viscous dissipation}}$$
$$+ \underbrace{\frac{RD}{C_\infty}\left(\frac{\partial C}{\partial r}\right)^2 + \frac{RD}{T_\infty}\left(\frac{\partial T}{\partial r}\right)\left(\frac{\partial C}{\partial r}\right)}_{\text{EG due to diffusion}} + \underbrace{\frac{\sigma B_0^2}{T_\infty}w^2}_{\text{EG due to magnetic field}} \qquad (15)$$

Eq. (15) reveals the four effects by which entropy is generated. The first effect is local volumetric entropy generation due to heat transfer across a finite temperature difference, is known as heat transfer irreversibility (HTI). The second effect is due to viscous dissipation and is known as fluid friction irreversibility (FFI). The third effect is due to diffusion or mass transfer across finite concentration difference and is known as diffusion irreversibility (DI). The fourth effect is due to magnetic field. The dimensionless entropy generation number Ns is defined as the ratio of local volumetric entropy generation S_{gen} and the characteristic entropy generation rate S_c. For the prescribed boundary conditions, the characteristic entropy generation rate is defined as

$$S_c = \frac{k(\Delta T)^2}{z^2 T_\infty^2}.$$

Thus the dimensionless entropy generation number can be defined as follows:

$$Ns = \frac{S_{gen}}{S_c}. \qquad (16)$$

Substituting the similarity transformation parameters and expressions of dimensionless velocity, temperature and concentration in Eq. (16), we obtain

$$Ns = (1 + 2\eta\gamma)Re\left[\theta'^2(\eta) + \frac{PrEc}{\Omega}f''^2(\eta) + \frac{\chi}{\Omega^2}\phi'^2(\eta)\right.$$
$$\left. + \frac{\chi}{\Omega}\theta'(\eta)\phi'(\eta) + \frac{M^2 Re}{\Omega}PrEc f'^2(\eta)\right], \qquad (17)$$
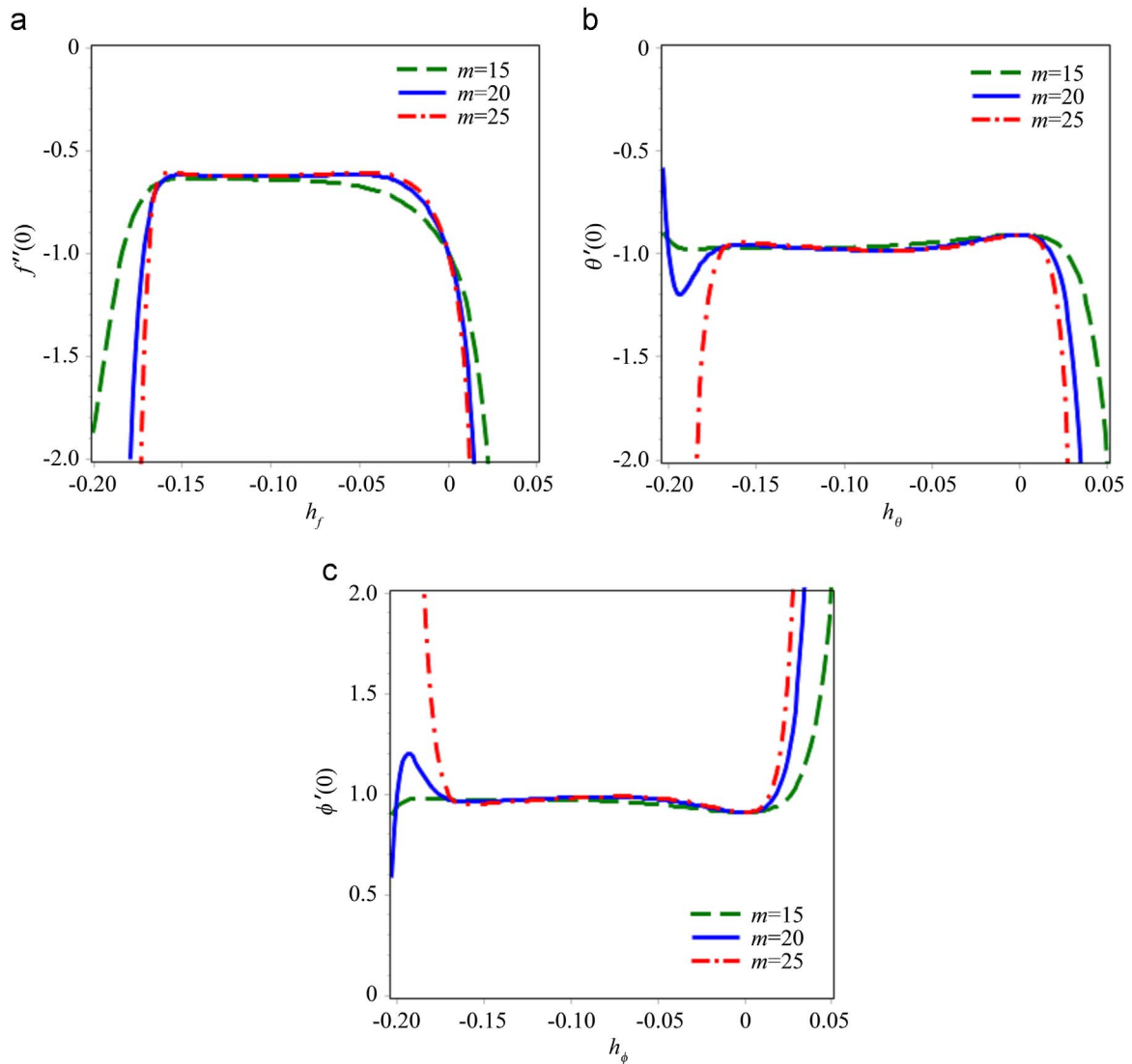
a

b

c

Figure 2 h-curves of $f''(0), \theta'(0)$ and $\phi'(0)$ for different order of approximations m.

where $\Omega = \frac{\Delta T}{T_\infty}$ is dimensionless temperature and $\chi = \frac{RDC_\infty}{k}$ is diffusive constant parameter.

4. Analytical solution via HAM

To derive analytical power series solutions for the transformed boundary value problem defined by Eqs. (8)-(10) under boundary conditions (11), the homotopy analysis method (HAM) is deployed. In this regard, we have selected the set of base functions $\{\eta^k \exp(-c\eta) | k \geq 0, c \geq 0\}$. The initial guesses and linear operators are chosen as follows [52]:

$$f_0(\eta) = \frac{1}{1 + \lambda_1 - \lambda_2}(1 - \exp(-\eta)), \ \theta_0(\eta) = \frac{1}{1 + \delta}\exp(-\eta),$$

$$\phi_0(\eta) = -\frac{Nt}{Nb}\exp(-\eta), 1 + \lambda_1 - \lambda_2 \neq 0, 1 + \delta \neq 0, \quad (18)$$

$$L_f(f) = \frac{\partial^3 f}{\partial \eta^3} + \frac{\partial^2 f}{\partial \eta^2}, \ L_\theta(\theta) = \frac{\partial^2 \theta}{\partial \eta^2} + \frac{\partial \theta}{\partial \eta}, \ L_\phi(\phi) = \frac{\partial^2 \phi}{\partial \eta^2}$$
$$+ \frac{\partial \phi}{\partial \eta}, \quad (19)$$

where L_f, L_θ and L_ϕ are satisfied the conditions

$$L_f(C_1 + C_2\eta + C_3 e^{-\eta}) = 0, \ L_\theta(C_4 + C_5 e^{-\eta}) = 0, \ L_\phi(C_6 + C_7 e^{-\eta}) = 0. \quad (20)$$

The zeroth order deformation equations are defined as:

$$(1 - q)L_f[\psi_f(\eta, q) - f_0(\eta)] = qh_f H_f(\eta)N_f \quad (21)$$

$$(1 - q)L_\theta[\psi_\theta(\eta, q) - \theta_0(\eta)] = qh_\theta H_\theta(\eta)N_\theta \quad (22)$$

Table 1 The values of $f'(0)$, $\theta(0)$ and $\{-\phi(0)\}$ for different order of approximations for the values of parameters $Nt=Nb=Nr=0.2$, $Sc=10$, $Ri=1$, $Ec=M=0.5$, $Pr=5$, $\gamma=\delta=\lambda_1=\lambda_2=0.1$.

Order	$f'(0)$	$\theta(0)$	$\{-\phi(0)\}$
10	0.9700	0.9272	0.2034
20	0.9648	0.9310	0.2171
30	0.9637	0.9314	0.2234
35	0.9636	0.9314	0.2245
40	0.9636	0.9314	0.2249
45	0.9636	0.9314	0.2249

Table 2 Comparison between the current analytical results and numerical results of $f'(0)$ and $\{-\theta'(0)\}$ for the values of parameters $Nt=Nb=Nr=0.2$, $Sc=10$, $Ri=1$, $M=0.5$, $\gamma=\delta=\lambda_1=\lambda_2=0.1$.

		$f'(0)$		$\{-\theta'(0)\}$	
Ec	Pr	HAM	Numerical	HAM	Numerical
0.1	1	0.9725	0.9726	0.5752	0.5750
	3	0.9610	0.9609	0.9618	0.9613
	5	0.9572	0.9569	1.2079	1.2075
0.3	1	0.9733	0.9734	0.5315	0.5314
	3	0.9623	0.9622	0.8184	0.8177
	5	0.9584	0.9582	0.9761	0.9763
0.5	1	0.9741	0.9642	0.4898	0.4896
	3	0.9636	0.9635	0.6851	0.6851
	5	0.9596	0.9594	0.7657	0.7663

$$(1-q)L_\phi[\psi_\phi(\eta,q)-\phi_0(\eta)]=qh_\phi H_\phi(\eta)N_\phi, \tag{23}$$

with boundary conditions

$$\psi_f(0,q)=0,\ \psi_f'(0,q)=1+\lambda_1\psi_f''(0,q)+\lambda_2\psi_f'''(0,q),\ \psi_f'(\infty,q)=0 \tag{24}$$

$$\psi_\theta(0,q)=1+\delta\psi_\theta'(0,q),\ \psi_\theta'(\infty,q)=0 \tag{25}$$

$$Nb\psi_\phi'(0,q)+Nt\psi_\theta'(0,q)=0,\ \psi_\phi'(\infty,q)=0. \tag{26}$$

In the above equations $q\in[0,1]$ is an embedding parameter, h_f, h_θ, h_ϕ are auxiliary parameters, H_f, H_θ, H_ϕ are auxiliary functions. Also, N_f, N_θ, N_ϕ are nonlinear operators, defined as:

$$N_f=(1+2\eta\gamma)\frac{\partial^3\psi_f}{\partial\eta^3}+2\gamma\frac{\partial^2\psi_f}{\partial\eta^2}-\left(\frac{\partial\psi_f}{\partial\eta}\right)^2-Nr\psi_\phi$$
$$+\psi_f\frac{\partial^2\psi_f}{\partial\eta^2}-M^2\frac{\partial\psi_f}{\partial\eta}+Ri\psi_\theta \tag{27}$$

$$N_\theta=\frac{1}{Pr}\left[(1+2\eta\gamma)\left(\frac{\partial^2\psi_\theta}{\partial\eta^2}+Nb\frac{\partial\psi_\theta}{\partial\eta}\frac{\partial\psi_\phi}{\partial\eta}\right)+2\gamma\frac{\partial\psi_\theta}{\partial\eta}\right]$$
$$+(1+2\eta\gamma)\left(Ec\left(\frac{\partial^2\psi_f}{\partial\eta^2}\right)^2+\frac{1}{Pr}Nt\left(\frac{\partial\psi_\theta}{\partial\eta}\right)^2\right)+\psi_f\frac{\partial\psi_\theta}{\partial\eta} \tag{28}$$

$$N_\phi=(1+2\eta\gamma)\left(\frac{\partial^2\psi_\phi}{\partial\eta^2}+\left(\frac{Nt}{Nb}\right)\frac{\partial^2\psi_\theta}{\partial\eta^2}\right)+2\gamma\frac{\partial\psi_\phi}{\partial\eta}$$
$$+2\left(\frac{Nt}{Nb}\right)\gamma\frac{\partial\psi_\theta}{\partial\eta}+Sc\psi_f\frac{\partial\psi_\phi}{\partial\eta}. \tag{29}$$

The Taylor's series expansions of $f(\eta,q)$, $\theta(\eta,q)$ and $\phi(\eta,q)$ with respect to q are:

$$f(\eta,q)=f_0(\eta)+\sum_{m=1}^{\infty}f_m(\eta)q^m$$

$$\theta(\eta,q)=\theta_0(\eta)+\sum_{m=1}^{\infty}\theta_m(\eta)q^m$$

$$\phi(\eta,q)=\phi_0(\eta)+\sum_{m=1}^{\infty}\phi_m(\eta)q^m$$

where:

Table 3 HAM values of $f''(0)$ and $-\theta'(0)$ for different values of Prandtl number Pr, buoyancy parameter Nr, thermophoresis parameter Nt, thermal slip parameter δ and second order slip parameter λ_2, whenever other parameters are fixed and the order (no. of terms) of approximation is 35.

|			$(\delta,\ \lambda_2)$					
			(0.1, 0.1)		(0.1, 0.2)		(0.2, 0.1)	
Pr	Nr	Nt	$-f''(0)$	$\{-\theta'(0)\}$	$-f''(0)$	$\{-\theta'(0)\}$	$-f''(0)$	$\{-\theta'(0)\}$
3	0.1	0.1	0.7086	0.7006	0.8016	0.6603	0.7347	0.6240
		0.25	0.6994	0.6785	0.7866	0.6403	0.7257	0.6065
		0.4	0.6902	0.6567	0.7717	0.6206	0.7166	0.5891
	0.1	0.1	0.7086	0.7006	0.8016	0.6603	0.7347	0.6240
	0.25		0.7050	0.7001	0.7928	0.6621	0.7315	0.6236
	0.4		0.7015	0.6995	0.7841	0.6639	0.7282	0.6231
5	0.1	0.1	0.7510	0.7808	0.8423	0.7148	0.7752	0.6754
		0.25	0.7427	0.7593	0.8278	0.6974	0.7672	0.6589
		0.4	0.7344	0.7379	0.8134	0.6800	0.7591	0.6424
	0.1	0.1	0.7510	0.7808	0.8423	0.7148	0.7752	0.6754
	0.25		0.7472	0.7802	0.8329	0.7185	0.7717	0.6750
	0.4		0.7434	0.7797	0.8234	0.7221	0.7683	0.6745
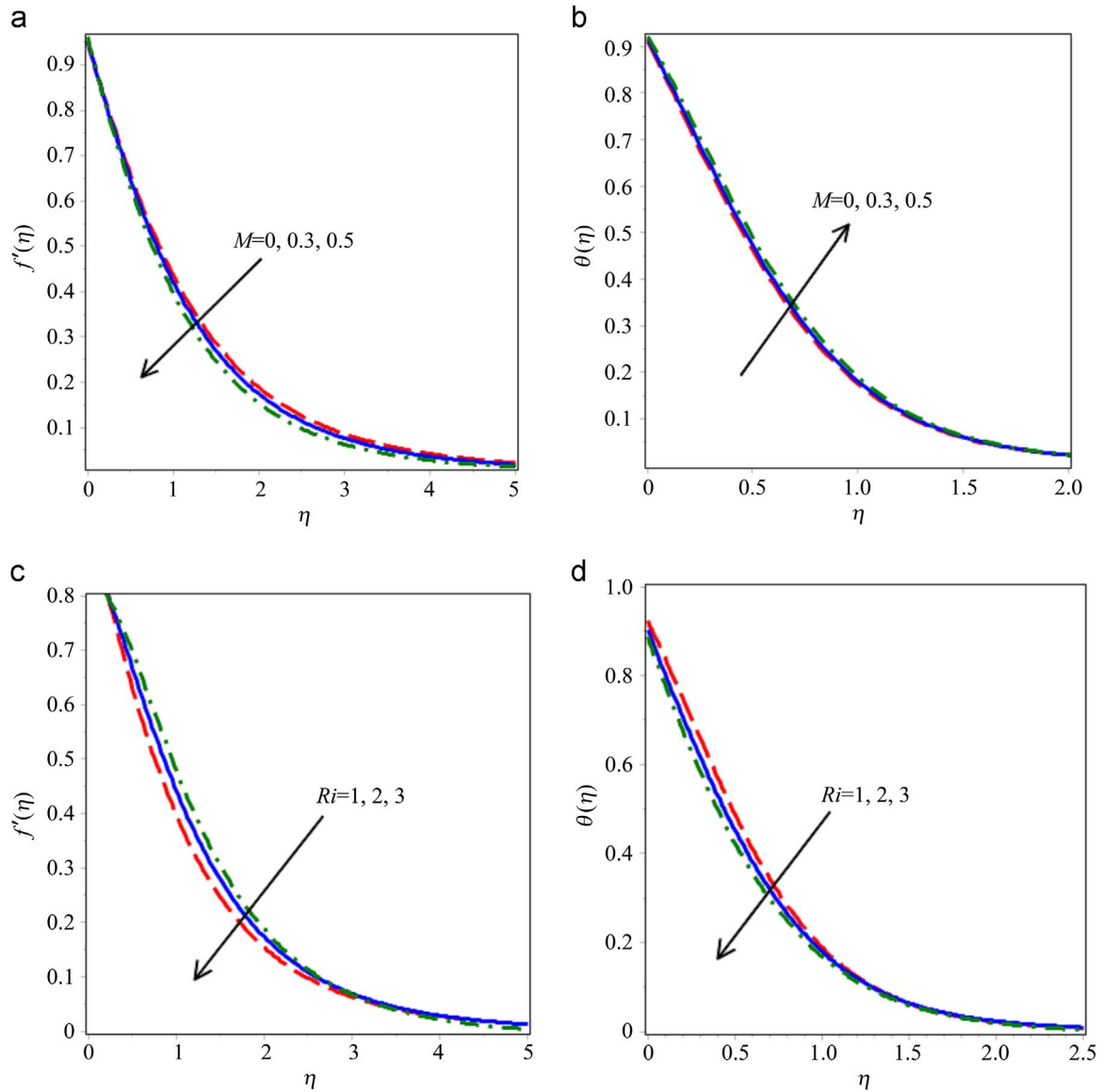
Figure 3   Effects of magnetic parameter M and mixed convection parameter Ri on velocity $f'(\eta)$ and temperature $\theta(\eta)$.

$$f_m = \frac{1}{m!}\frac{\partial^m \psi_f(\eta,q)}{\partial q^m}\Big|_{q=0},\ \theta_m = \frac{1}{m!}\frac{\partial^m \psi_\theta(\eta,q)}{\partial q^m}\Big|_{q=0}$$

$$\text{and}\quad \phi_m = \frac{1}{m!}\frac{\partial^m \psi_\phi(\eta,q)}{\partial q^m}\Big|_{q=0}. \tag{30}$$

On differentiating Eqs. (21), (22) and (23) m times with respect to q and dividing these by $m!$ and then substitute $q = 0$, we obtain the mth order deformation equations, which are defined as:

$$L_f(f_m(\eta) - \chi_{m-1}f_{m-1}(\eta)) = h_f H_f R_m^f(\eta) \tag{31}$$

$$L_\theta(\theta_m(\eta) - \chi_{m-1}\theta_{m-1}(\eta)) = h_\theta H_\theta R_m^\theta(\eta) \tag{32}$$

$$L_\phi(\phi_m(\eta) - \chi_{m-1}\phi_{m-1}(\eta)) = h_\phi H_\phi R_m^\phi(\eta) \tag{33}$$

$$f_m(0) = 0,\ f'_m(0) - \lambda_1 f''_m(0) - \lambda_2 f'''_m(0) = 0,\ f'_m(\infty) = 0 \tag{34}$$

$$\theta_m(0) - \delta\theta'_m(0) = 0,\ \theta(\infty) = 0 \tag{35}$$

$$Nb\phi'(0) + Nt\theta'(0) = 0 \tag{36}$$

where

$$R_m^f(\eta) = \frac{1}{m-1!}\frac{\partial^{m-1}N_f}{\partial q^{m-1}}\Big|_{q=0}$$

$$= (1 + 2\eta\gamma)f'''_{m-1} + 2\gamma f''_{m-1} - M^2 f'_{m-1}$$

$$+ Ri[\theta_{m-1} - Nr\phi_{m-1}] + \sum_{i=0}^{m-1}(f'_i f'_{m-1-i} + f_i f''_{m-1-i}) \tag{37}$$

$$R_m^\theta(\eta) = \frac{1}{m-1!} \frac{\partial^{m-1} N_\theta}{\partial q^{m-1}}\bigg|_{q=0}$$

$$= \frac{1}{Pr}\left[(1+2\eta\gamma)(\theta''_{m-1} + \sum_{i=0}^{m-1}(Nb\theta'_i\phi'_{m-1-i}\right.$$

$$+ Nt\theta'_i\theta'_{m-1-i})) + 2\gamma\theta'_{m-1}\bigg]$$

$$+ (1+2\eta\gamma)Ec\sum_{i=0}^{m-1}f''_if''_{m-1-i} + \sum_{i=0}^{m-1}f_i\theta'_{m-1-i} \qquad (38)$$

$$R_m^\phi(\eta) = \frac{1}{m-1!}\frac{\partial^{m-1}N_\phi}{\partial q^{m-1}}\bigg|_{q=0}$$

$$= (1+2\eta\gamma)\phi''_{m-1} + 2\gamma\phi'_{m-1} + 2\left(\frac{Nt}{Nb}\right)\gamma\theta'_{m-1}$$

$$+ (1+2\eta\gamma)\left(\frac{Nt}{Nb}\right)\theta''_{m-1} + Sc\sum_{i=0}^{m-1}f_i\theta'_{m-1-i} \qquad (39)$$

and $\quad \chi_m = \begin{cases} 0, & m \le 1 \\ 1, & m > 1 \end{cases}.$

We have solved the Eqs. (31)-(33) with the help of the symbolic software Maple 18 and obtained the mth term in following form

$$f_m(\eta) = F_m(\eta) + C_1 + C_2\eta + C_3e^{-\eta} \qquad (40)$$

$$\theta_m(\eta) = \Theta_m(\eta) + C_4 + C_5e^{-\eta} \qquad (41)$$

$$\phi_m(\eta) = \Phi_m(\eta) + C_6 + C_7e^{-\eta}. \qquad (42)$$

Here $F_m(\eta)$, $\Theta_m(\eta)$ and $\Phi_m(\eta)$ are the particular solutions and C_1 to C_7 are the constants which can be calculated with the help of the Eqs. (34)-(36).

Thus, the analytical series solutions of $f(\eta)$, $\theta(\eta)$ and $\phi(\eta)$ are given as follows:

$$f(\eta) = f_0(\eta) + \sum_{m=1}^{\infty} f_m(\eta), \qquad (43)$$

$$\theta(\eta) = \theta_0(\eta) + \sum_{m=1}^{\infty} \theta_m(\eta), \qquad (44)$$

$$\phi(\eta) = \phi_0(\eta) + \sum_{m=1}^{\infty} \phi_m(\eta) \qquad (45)$$

5. Convergence discussion of HAM

Liao [45] pointed that the rate of approximations and convergence of HAM solution is strongly dependent on auxiliary parameters h_f, h_θ and h_ϕ. To find out the appropriate values of h_f, h_θ and h_ϕ, we have plotted h-curves with $f''(0)$, $\theta'(0)$ and $\phi'(0)$ for different order of approximations, which display in Figures 2(a)-(c). The adequate ranges for h_f, h_θ and h_ϕ are $[-0.07, -0.15]$, $[-0.08, -0.16]$ and $[-0.08, -0.16]$ respectively. Table 1 represents the convergence of series of solutions up to 45th order of approximations for the values of auxiliary parameters $h_f = h_\theta = h_\phi = -0.125$ and it has been observed that the series are convergent up to 35th order of approximations.

6. Numerical validation

To check the accuracy of HAM, the present analytic results have been compared with numerical results, which are presented in Table 2. This table represents a good agreement between the both results for the same values of
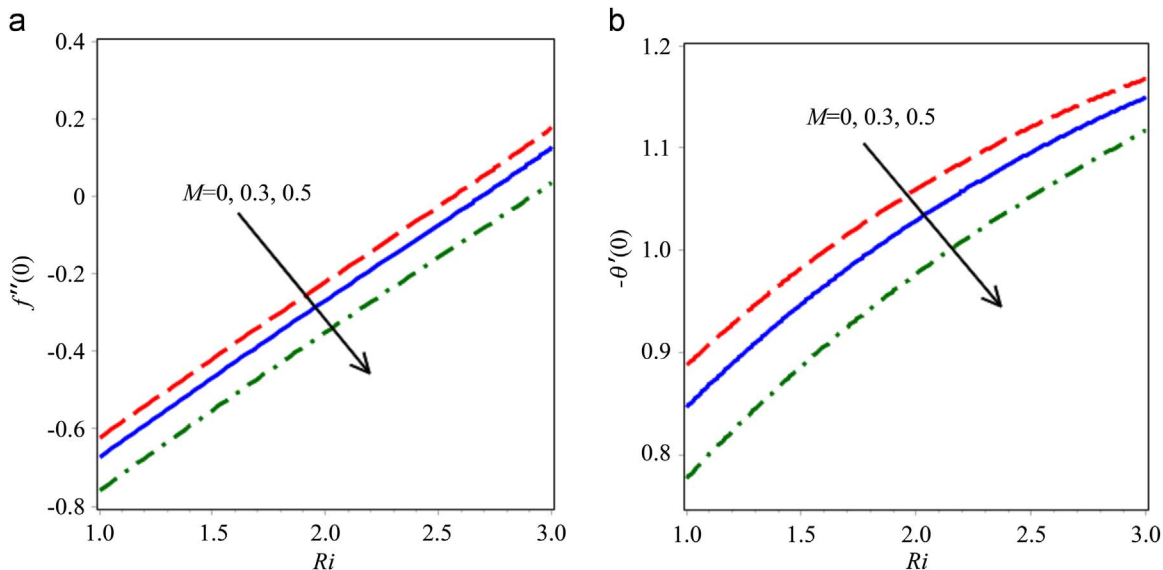

Figure 4 Effects of magnetic parameter M and mixed convection parameter Ri on skin friction coefficient $f''(0)$ and rate of heat transfer $\{-\theta'(0)\}$.

auxiliary parameters $h_f = h_\theta = h_\phi = -0.125$, which are used in Table 1 on 35th order of approximations. Thus, we have used the values as optimum values. The numerical validation has been done by using RKF45 with shooting technique by converting into initial value problem. The system of first order differential equations is created by assuming $(f, f', f'', \theta, \theta', \phi, \phi') = (U_1, U_2, U_3, U_4, U_5, U_6, U_7)$, as given below

$$
\begin{pmatrix} U_1' \\ U_2' \\ U_3' \\ U_4' \\ U_5' \\ U_6' \\ U_7' \end{pmatrix} = \begin{pmatrix} U_2 \\ U_3 \\ \frac{1}{1+2\eta\gamma}\left[-Ri(U_4 - NrU_6) + U_2^2 + M^2 U_2 - 2\gamma U_3 - U_1 U_3\right] \\ U_5 \\ -\left[\frac{Pr}{1+2\eta\gamma}U_1 U_5 + \frac{2\gamma}{1+2\eta\gamma}U_5 + PrEcU_3^2 + NbU_5 U_7 + NtU_5^2\right] \\ U_7 \\ \frac{-1}{1+2\eta\gamma}\left[2\gamma U_7 + ScU_1 U_7 + 2\frac{Nt}{Nb}\gamma U_5\right] - \frac{Nt}{Nb}U_5' \end{pmatrix},
$$

With $\left(0, 1 + \lambda_1 U_3 + \lambda_2 U_3', U_3, 1 + \delta U_5, U_5, U_6, -\frac{Nt}{Nb}U_5\right)^T$.

The initial values for $f''(0)$, $\theta'(0)$ and $\phi(0)$ are chosen, such that far-field conditions i.e. $f'(\infty) = 0$, $\theta(\infty) = 0$, $\phi(\infty) = 0$, are satisfied with appropriate domain length η_∞ and update these values iteratively till the convergence criterion attained.

7. Results and discussion

The coupled system of nonlinear ordinary differential Eqs. (8)-(10) with boundary conditions (11) has been solved by applying homotopy analysis method. Extensive computations have been conducted to elaborate the influence of key physical parameters (i.e. magnetic parameter M, curvature parameter γ, first and second order velocity slip parameters λ_1 & λ_2, thermal slip parameter δ and Richardson number Ri on the significant physical quantities i.e. velocity $f'(\eta)$, skin fiction coefficient $f''(0)$, temperature $\theta(\eta)$, rate of heat transfer and entropy generation number Ns. For all the computations reported herein, the default values of governing parameters are taken as $Nt = Nb = Nr = 0.2$, $Sc = 10$, $Ri = 1$, $Ec = M = 0.5$, $Pr = 5$, $\lambda_1 = \lambda_2 = 0.1$, $\gamma = \delta = 0.1$, otherwise mentioned. The HAM values of $f''(0)$ and $\{-\theta'(0)\}$ are presented in Table 3 for different values of Pr, Nt, Nr, δ and λ_2 whereas others parameters are fixed. Table 3 shows that skin friction coefficient $f''(0)$ and rate of heat transfer $\{-\theta'(0)\}$ are increasing with an increase in value of Prandtl number Pr whereas a reduction in both skin friction and rate of heat transfer is observed as thermophoresis parameter Nt increases.

The skin friction is lower for increasing values of buoyancy parameter Nr, as are the values of heat transfer rate $\{-\theta'(0)\}$. As we increase the value of second order slip parameter λ_2 from 0.1 to 0.2, the rate of heat transfer $\{-\theta'(0)\}$ decreases with increasing value of buoyancy parameter Nr for $\lambda_2 = 0.1$, whereas the reverse trend is observed for higher values of second order slip ($\lambda_2 > 0.12$ approximately). Figure 3(a)-(b) present the effect of
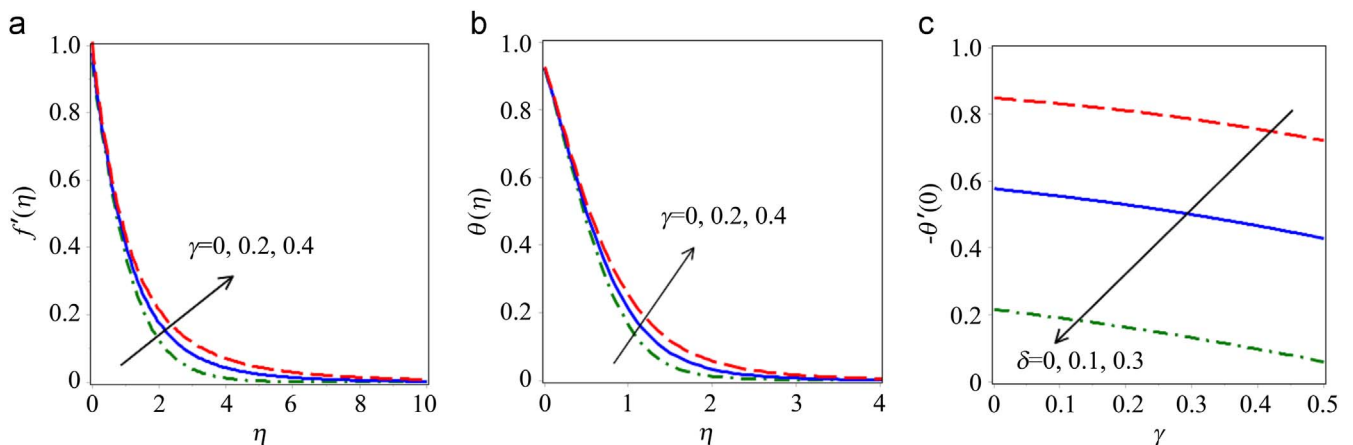

Figure 5 Effects of curvature parameter γ on velocity $f'(\eta)$ and temperature $\theta(\eta)$ and combined effects of thermal slip parameter δ and curvature parameter γ on rate of heat transfer.

magnetic parameter M and Figure 3(c)-(d) represent the effect of Richardson number Ri on velocity and temperature respectively. It has been observed that velocity decreases but temperature increases with greater magnetic parameter. This is attributable to the fact that as magnetic field increases, momentum development is inhibited owing to the retarding nature of the Lorentz magnetic body force effect. This decelerates the nanofluid flow and increases momentum boundary layer thickness. Furthermore increasing magnetic field has the tendency to increase the temperature of nanofluid flow since supplementary work expended in dragging the nanofluid against the action of the magnetic field is dissipated as thermal energy. Stronger magnetic field therefore enhances thermal boundary layer thickness. Lower values of $Ri(\ll 1)$ correspond to natural convection and higher values of $Ri(\gg 10)$ indicate forced convection. When Ri falls between 1 to 10 this represents mixed convection. Thus, we have used $Ri = 1$, 2 and 3, since the present study focuses on the effect of mixed convection on nanofluid flow. With increasing Richardson number, both velocity and temperatures are suppressed in the regime. Generally deceleration and cooling of the nanofluid boundary layer are therefore induced with higher Richardson number. Momentum boundary layer is increased and thermal boundary layer thickness is decreased.

The effects of magnetic parameter M and Richardson number Ri on skin friction coefficient and heat transfer rate are shown in Figure 4(a)-(b). Both physical quantities decrease with magnetic parameter whereas they increase with mixed convection parameter. These are consistent with the earlier observations regarding velocity and temperature behavior (Figure 3(a)-(d)). Figure 5(a)-(b) show that
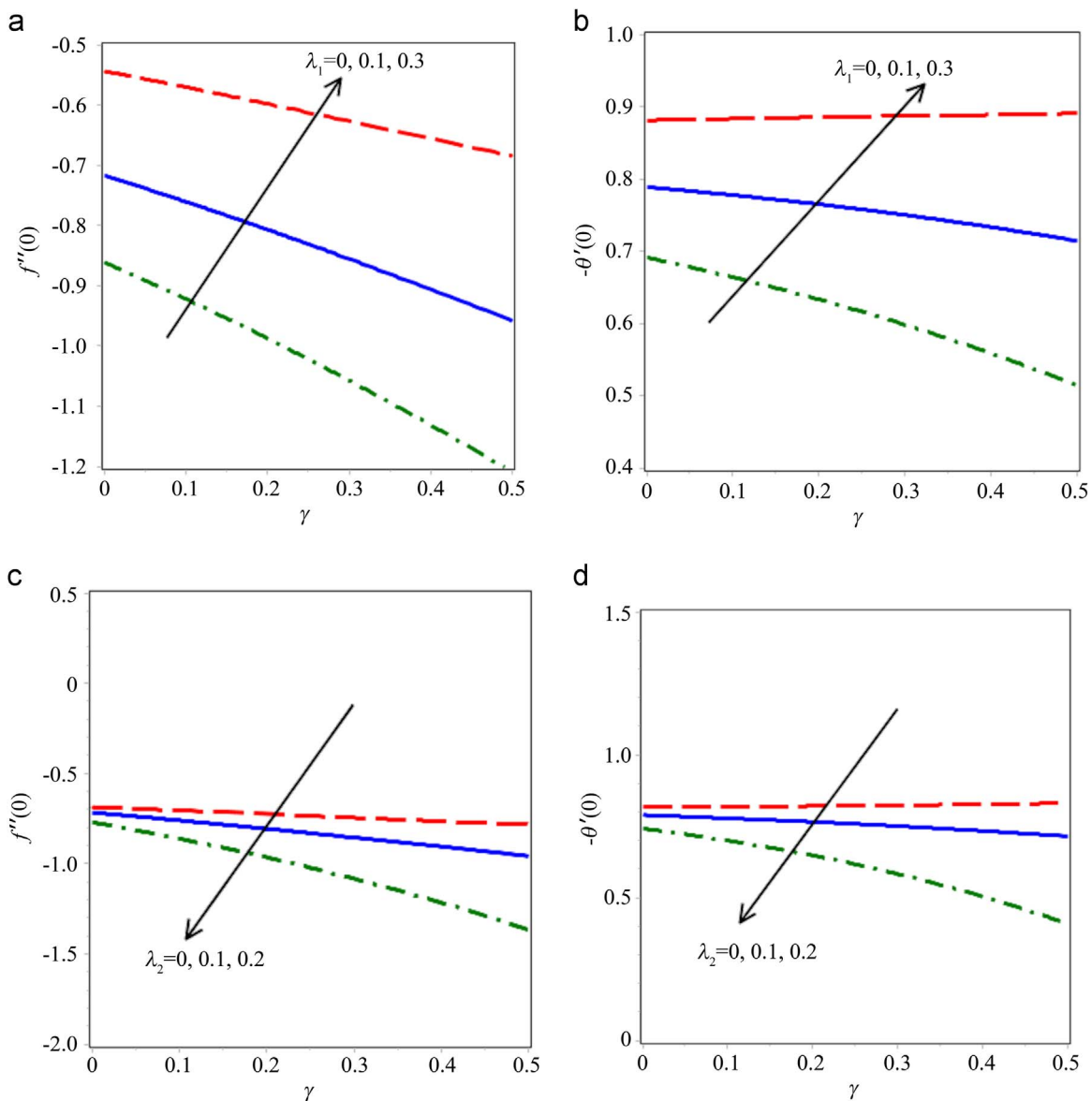

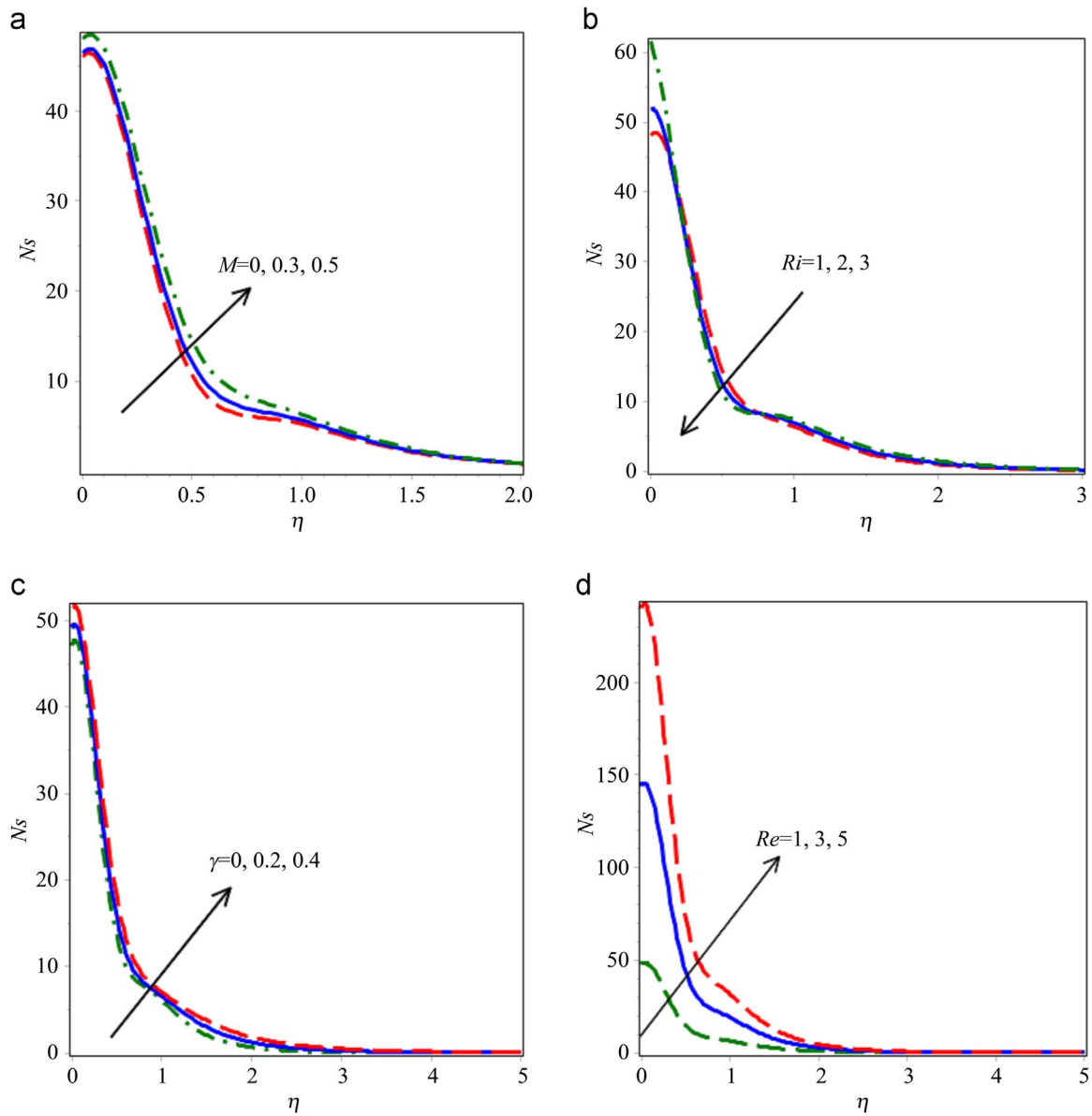Figure 6   Effects of first and second order velocity slip parameter λ_1 & λ_2 on $f''(0)$ and $\{-\theta'(0)\}$.

Figure 7   Effects of M, Ri, γ and Re on entropy generation number Ns.
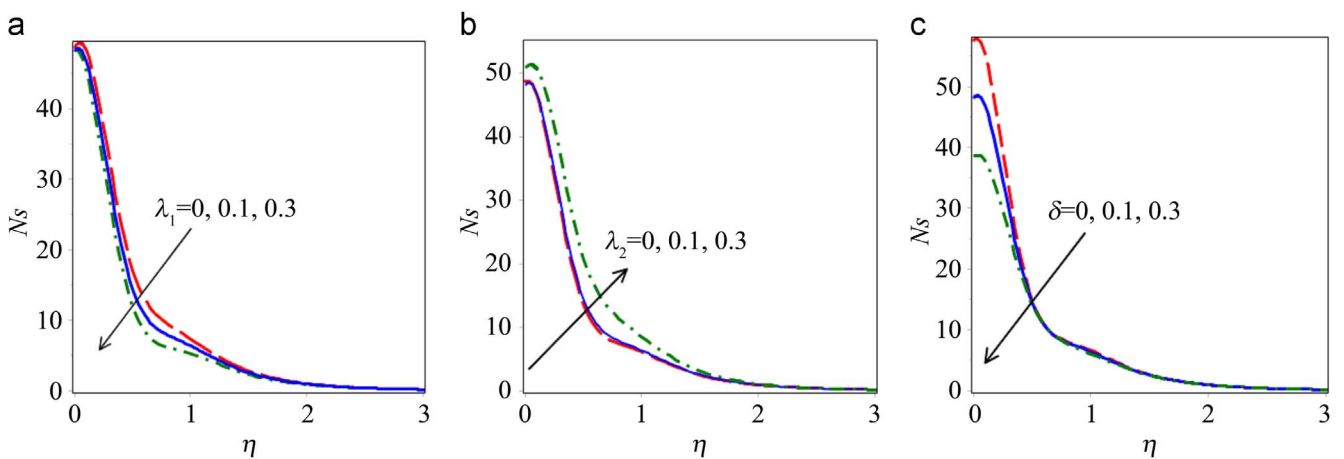
Figure 8   Effects of slip parameters (first and second order velocity slip λ_1 & λ_2) and thermal slip parameter δ on entropy.
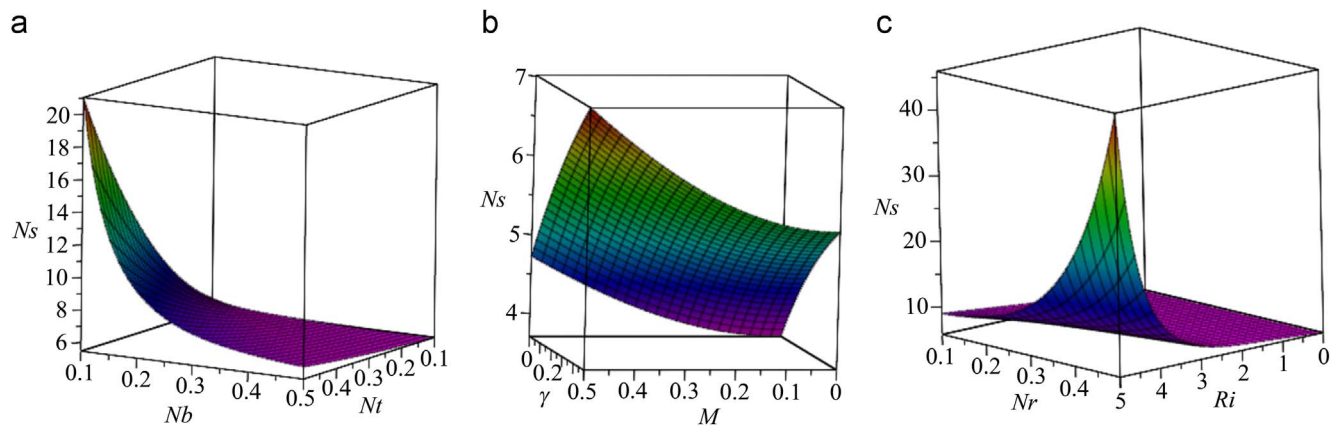
a

b

c

Figure 9 Combined effects of (Nt, Nb), (M, γ) and (Ri, Nr) on entropy generation number Ns.

increasing curvature parameter γ enhances both velocity and temperature *i.e.* accelerates and simultaneously heats the boundary layer flow. Velocity and temperature are therefore minimal in the absence of curvature effect. The combined effects of curvature parameter γ and thermal slip parameter δ on the rate of heat transfer are presented in Figure 5(c). It is evident that heat transfer rate is decreased with curvature parameter (since temperatures in the boundary layer are enhanced and less heat is convected to the cylinder surface). Additionally with increasing thermal slip there is a reduction in heat transfer rate. Heat transfer rate is therefore a maximum when thermal slip effect is absent. Figure 6(a)-(d), present the effects of first and second order velocity slip parameters λ_1 & λ_2 and curvature parameter γ on skin friction coefficient and rate of heat transfer. Both skin friction and heat transfer rate at the cylinder wall are elevated with first order slip effect. Conversely, both skin friction and heat transfer rate are depressed with increasing second order slip λ_2 and cylinder curvature parameter γ. The influence of thermal slip is however much stronger than curvature parameter. Nevertheless the computations do confirm that curvature effects should not be ignored in external boundary layer convection from curved bodies.

Figures 7 and 8 examine the influence of governing parameters M, Ri, γ, Re, λ_1, λ_2 & δ on the entropy generation number Ns. We have observed that entropy increases close to the cylinder surface whereas it demonstrates the opposite behavior with an increasing value of η. Therefore near the wall of cylinder greater entropy is generated. At the cylinder surface, a significant amount of energy is dissipated which is associated with both Eckert and magnetic parameters. Figure 7(a) illustrates that entropy increases with increasing values of magnetic parameter M, since magnetic field enhances the temperatures in the boundary layer. The effect of mixed convection parameter Ri is presented in Figure 7(b). It has been observed that entropy generation number Ns is

lesser for higher values of Ri in the vicinity of surface whereas the converse trend is noted further from the cylinder surface i.e. as η increases. Figures 7(c)-(d) depict the effects of curvature parameter γ and Reynolds number Re on entropy generation number Ns. Apparently entropy increases with both parameters. Effectively more curved bodies create greater quantities of entropy. Reynolds number increases the entropy since this number is ratio of inertia force to the viscous force. A higher value of Reynolds number, even if laminar (Re is varied from 1 to 5), implies acceleration in the flow, which encourages disorder in fluid movement.

The effects of first and second order velocity slip and thermal slip parameters i.e. λ_1, λ_2 & δ on entropy generation number Ne are presented in Figure 8(a)-(c). Entropy decreases with increment in λ_1 whereas it is enhanced with increasing value of λ_2. Higher order velocity slip therefore encourages entropy generation in the nanofluid. Figure 8(c) indicates that near the cylinder surface, entropy increases with an increasing the value of thermal slip δ whereas with further penetration into the boundary layer, the influence is negligible. This is associated with the fact that temperature has higher values near the surface of cylinder and this maximizes the thermal slip effect in this zone. Thermal slip is also applied as a boundary condition on the cylinder surface and it is entirely logical that the influence will be progressively depleted and eventually vanishes with distance from the cylinder surface. We have analyzed the combined effects of physical parameters (Nt, Nb), (M, γ) and (Ri, Nr) on the entropy generation number Ns at $\eta = 1$. These are illustrated in Figure 9(a)-(c). Figure 9(a) demonstrates that Ns increases with thermophoresis parameter Nt whereas it decreases with Brownian motion parameter Nb (i.e. for smaller sized nanoparticles). Increasing Brownian motion of nanoparticles therefore inhibits entropy generation in the system. Figure 9(b) indicates that entropy generation increases with an increment in the value of magnetic and curvature parameters which is consistent with the results of Figure 7(a)-(c).

The combined effects of mixed convection parameter Ri and buoyancy parameter Nr are depicted in Figure 9(c) which shows that entropy generation number increases with both these parameters. With increasing buoyancy effect, entropy generation is enhanced in the nanofluid regime.

8. Conclusions

In the current article, an analytical study of entropy generation in magnetohydrodynamic dissipative mixed convection nanofluid flow over a vertical cylinder has been presented. Both first and second order velocity slip and also thermal slip effects have been considered at the cylinder surface. The homotopy analysis method (HAM) has been applied to solve the transformed, non-dimensional, coupled system of nonlinear ordinary differential equations for momentum, energy (heat) and species (nano-particle) conservation subject to physically viable boundary conditions. The effects of first and second order velocity slip parameters (λ_1, λ_2), mixed convection parameter i.e. Richardson number (Ri), magnetic parameter (M), curvature parameter (γ) and thermal slip parameter (δ) on velocity $f'(\eta)$, skin friction coefficient $f''(0)$ and also temperature $\theta(\eta)$, rate of heat transfer $\left\{ -\theta'(0) \right\}$ and entropy generation number (Ns) have been evaluated in detail. The current computations have demonstrated that:

- Nanofluid velocity decreases with magnetic parameter whereas it increases with curvature parameter.
- The flow is accelerated with increasing mixed convection parameter near the leading edge of the cylinder whereas the reverse effect is observed further from the cylinder surface.
- Increasing both magnetic parameter and second order velocity slip parameter reduces the skin friction coefficient.
- Increasing mixed convection parameter, curvature parameter and first order velocity slip parameter enhances skin friction.
- Temperature increases with greater curvature parameter and magnetic parameter but decreases with higher values of mixed convection parameter.
- The rate of heat transfer decreases with increasing magnetic parameter, second order velocity slip parameter and thermal slip parameter whereas it is elevated with greater mixed convection parameter, curvature parameter and first order velocity slip parameter.
- Entropy generation is enhanced with magnetic parameter, second order slip velocity parameter, curvature parameter, thermophoresis parameter, buoyancy parameter and Reynolds number.
- Entropy generation is reduced with increasing first order velocity slip parameter, Brownian motion parameter and thermal slip parameter. However the influence of mixed convection parameter (Richardson number) may either enhance or reduce the entropy generation depending on the location relative to the cylinder surface i.e. there is a variable behaviour in entropy generation with mixed convection parameter.

References

[1] S.U.S. Choi, J.A. Eastman, Enhancing Thermal Conductivity of Fluids with Nanoparticles, Argonne National Lab., IL (United States), 1995 ⟨https://www.osti.gov/scitech/biblio/196525/⟩ (Accessed 28 March 2017).

[2] R. Saidur, K.Y. Leong, H.A. Mohammad, A review on applications and challenges of nanofluids, Renew. Sustain. Energy Rev. 15 (2011) 1646–1668, https://doi.org/10.1016/j.rser.2010.11.035.

[3] M. Sheikholeslami, Influence of Coulomb forces on Fe_3O_4-H_2O nanofluid thermal improvement, Int. J. Hydrog. Energy 42 (2017) 821–829, https://doi.org/10.1016/j.ijhydene.2016.09.185.

[4] M. Sheikholeslami, H.B. Rokni, Melting heat transfer influence on nanofluid flow inside a cavity in existence of magnetic field, Int. J. Heat Mass Transf. 114 (2017) 517–526, https://doi.org/10.1016/j.ijheatmasstransfer.2017.06.092.

[5] J. Buongiorno, Convective transport in nanofluids, ASME J. Heat Transf. 128 (2006) 240–250, https://doi.org/10.1115/1.2150834.

[6] M. Sheikholeslami, H.B. Rokni, Nanofluid two phase model analysis in existence of induced magnetic field, Int. J. Heat Mass Transf. 107 (2017) 288–299, https://doi.org/10.1016/j.ijheatmasstransfer.2016.10.130.

[7] P. Rana, R. Dhanai, L. Kumar, MHD slip flow and heat transfer of Al_2O_3-water nanofluid over a horizontal shrinking cylinder using Buongiorno's model: effect of nanolayer and nanoparticle diameter, Adv. Powder Technol. 28 (2017) 1727–1738, https://doi.org/10.1016/j.apt.2017.04.010.

[8] M. Sheikholeslami, A. Zeeshan, Analysis of flow and heat transfer in water based nanofluid due to magnetic field in a porous enclosure with constant heat flux using CVFEM, Comput. Methods Appl. Mech. Eng. 320 (2017) 68–81, https://doi.org/10.1016/j.cma.2017.03.024.

[9] S. Heysiattalab, A. Malvandi, D.D. Ganji, Anisotropic behavior of magnetic nanofluids (MNFs) at filmwise condensation over a vertical plate in presence of a uniform variable-directional magnetic field, J. Mol. Liq. 219 (2016) 875–882, https://doi.org/10.1016/j.molliq.2016.04.004.

[10] A. Malvandi, S. Heysiattalab, D.D. Ganji, Effects of magnetic field strength and direction on anisotropic thermal conductivity of ferrofluids (magnetic nanofluids) at filmwise condensation over a vertical cylinder, Adv. Powder Technol. 27 (2016) 1539–1546, https://doi.org/10.1016/j.apt.2016.05.015.

[11] A.M. Rashad, Impact of thermal radiation on MHD slip flow of a ferrofluid over a non-isothermal wedge, J. Magn. Magn. Mater. 422 (2017) 25–31, https://doi.org/10.1016/j.jmmm.2016.08.056.

[12] S. Sivasankaran, M.A. Mansour, A.M. Rashad, M. Bhuvaneswari, MHD mixed convection of Cu-water nanofluid in a two-sided lid-driven porous cavity with a partial slip, Numer. Heat Transf. Part Appl. 70 (2016) 1356–1370, https://doi.org/10.1080/10407782.2016.1243957.

[13] M.A. Ismael, M.A. Mansour, A.J. Chamkha, A.M. Rashad, Mixed convection in a nanofluid filled-cavity with partial slip subjected to constant heat flux and inclined magnetic field, J.

Magn. Magn. Mater. 416 (2016) 25–36, https://doi.org/10.1016/j.jmmm.2016.05.006.

[14] A.V. Kuznetsov, D.A. Nield, Natural convective boundary-layer flow of a nanofluid past a vertical plate: a revised model, Int. J. Therm. Sci. 77 (2014) 126–129, https://doi.org/10.1016/j.ijthermalsci.2013.10.007.

[15] A. Aziz, W.A. Khan, Natural convective boundary layer flow of a nanofluid past a convectively heated vertical plate, Int. J. Therm. Sci. 52 (2012) 83–90, https://doi.org/10.1016/j.ijthermalsci.2011.10.001.

[16] M. Sheikholeslami, Numerical simulation of magnetic nanofluid natural convection in porous media, Phys. Lett. A 381 (2017) 494–503, https://doi.org/10.1016/j.physleta.2016.11.042.

[17] M. Sheikholeslami, CuO-water nanofluid free convection in a porous cavity considering Darcy law, Eur. Phys. J. 132 (2017) 55, https://doi.org/10.1140/epjp/i2017-11330-3.

[18] M. Sheikholeslami, Lattice Boltzmann method simulation for MHD non-Darcy nanofluid free convection, Phys. B Condens. Matter 516 (2017) 55–71, https://doi.org/10.1016/j.physb.2017.04.029.

[19] M. Sheikholeslami, H.B. Rokni, Magnetic nanofluid natural convection in the presence of thermal radiation considering variable viscosity, Eur. Phys. J. 132 (2017) 238, https://doi.org/10.1140/epjp/i2017-11498-4.

[20] S.E. Mahgoub, Forced convection heat transfer over a flat plate in a porous medium, Ain Shams Eng. J. 4 (2013) 605–613, https://doi.org/10.1016/j.asej.2013.01.002.

[21] M. Hatami, R. Nouri, D.D. Ganji, Forced convection analysis for MHD Al_2O_3-water nanofluid flow over a horizontal plate, J. Mol. Liq. 187 (2013) 294–301, https://doi.org/10.1016/j.molliq.2013.08.008.

[22] M. Sheikholeslami, Magnetohydrodynamic nanofluid forced convection in a porous lid driven cubic cavity using Lattice Boltzmann method, J. Mol. Liq. 231 (2017) 555–565, https://doi.org/10.1016/j.molliq.2017.02.020.

[23] M. Sheikholeslami, Influence of magnetic field on nanofluid free convection in an open porous cavity by means of Lattice Boltzmann method, J. Mol. Liq. 234 (2017) 364–374, https://doi.org/10.1016/j.molliq.2017.03.104.

[24] R. Nazar, L. Tham, I. Pop, D.B. Ingham, Mixed convection boundary layer flow from a horizontal circular cylinder embedded in a porous medium filled with a nanofluid, Transp. Porous Media 86 (2011) 517–536, https://doi.org/10.1007/s11242-010-9637-1.

[25] P. Rana, R. Bhargava, O.A. Bég, Finite element modeling of conjugate mixed convection flow of Al_2O_3-water nanofluid from an inclined slender hollow cylinder, Phys. Scr. 87 (2013) 1–15, https://doi.org/10.1088/0031-8949/87/05/055005.

[26] R. Trîmbiţaş, T. Grosan, I. Pop, Mixed convection boundary layer flow past vertical flat plate in nanofluid: case of prescribed wall heat flux, Appl. Math. Mech. 36 (2015) 1091–1104, https://doi.org/10.1007/s10483-015-1967-7.

[27] A. Yoshimura, R.K. Prud'homme, Wall slip corrections for couette and parallel disk viscometers, J. Rheol. 32 (1988) 53–67, https://doi.org/10.1122/1.549963.

[28] H.I. Andersson, Slip flow past a stretching surface, Acta Mech. 158 (2002) 121–125, https://doi.org/10.1007/BF01463174.

[29] P. Rana, M.J. Uddin, Y. Gupta, A.I.M. Ismail, Slip effects on MHD Hiemenz stagnation point nanofluid flow and heat transfer along a nonlinearly shrinking sheet with induced magnetic field: multiple solutions, J. Braz. Soc. Mech. Sci.

Eng. 39 (2017) 3363–3374, https://doi.org/10.1007/s40430-017-0730-z.

[30] L. Zheng, C. Zhang, X. Zhang, J. Zhang, Flow and radiation heat transfer of a nanofluid over a stretching sheet with velocity slip and temperature jump in porous medium, J. Frankl. Inst. 350 (2013) 990–1007, https://doi.org/10.1016/j.jfranklin.2013.01.022.

[31] R. Dhanai, P. Rana, L. Kumar, MHD mixed convection nanofluid flow and heat transfer over an inclined cylinder due to velocity and thermal slip effects: Buongiorno's model, Powder Technol. 288 (2016) 140–150, https://doi.org/10.1016/j.powtec.2015.11.004.

[32] R. Dhanai, P. Rana, L. Kumar, Lie group analysis for bioconvection MHD slip flow and heat transfer of nanofluid over an inclined sheet: multiple solutions, J. Taiwan Inst. Chem. Eng. 66 (2016) 283–291, https://doi.org/10.1016/j.jtice.2016.07.001.

[33] P. Rana, R. Dhanai, L. Kumar, Radiative nanofluid flow and heat transfer over a non-linear permeable sheet with slip conditions and variable magnetic field: dual solutions, Ain Shams Eng. J. 8 (2017) 341–352, https://doi.org/10.1016/j.asej.2015.08.016.

[34] L. Wu, A slip model for rarefied gas flows at arbitrary Knudsen number, Appl. Phys. Lett. 93 (2008) 253103, https://doi.org/10.1063/1.3052923.

[35] T. Fang, S. Yao, J. Zhang, A. Aziz, Viscous flow over a shrinking sheet with a second order slip flow model, Commun. Nonlinear Sci. Numer. Simul. 15 (2010) 1831–1842, https://doi.org/10.1016/j.cnsns.2009.07.017.

[36] J. Zhu, L. Zheng, L. Zheng, X. Zhang, Second-order slip MHD flow and heat transfer of nanofluids with thermal radiation and chemical reaction, Appl. Math. Mech. 36 (2015) 1131–1146, https://doi.org/10.1007/s10483-015-1977-6.

[37] R. Sharma, A. Ishak, Second order slip flow of cu-water nanofluid over a stretching sheet with heat transfer, WSEAS Trans. Fluid Mech. 9 (2014) 26–33.

[38] F. Mabood, A. Mastroberardino, Melting heat transfer on MHD convective flow of a nanofluid over a stretching sheet with viscous dissipation and second order slip, J. Taiwan Inst. Chem. Eng. 57 (2015) 62–68, https://doi.org/10.1016/j.jtice.2015.05.020.

[39] A. Bejan, A study of entropy generation in fundamental convective heat transfer, J. Heat Transf. 101 (1979) 718–725, https://doi.org/10.1115/1.3451063.

[40] A. Bejan, Method of entropy generation minimization, or modeling and optimization based on combined heat transfer and thermodynamics, Rev. Générale Therm. 35 (1996) 637–646, https://doi.org/10.1016/S0035-3159(96)80059-6.

[41] S. Aïboud, S. Saouli, Second law analysis of viscoelastic fluid over a stretching sheet subject to a transverse magnetic field with heat and mass transfer, Entropy 12 (2010) 1867–1884, https://doi.org/10.3390/e12081867.

[42] M.H. Abolbashari, N. Freidoonimehr, F. Nazari, M.M. Rashidi, Analytical modeling of entropy generation for Casson nano-fluid flow induced by a stretching surface, Adv. Powder Technol. 26 (2015) 542–552, https://doi.org/10.1016/j.apt.2015.01.003.

[43] A. Noghrehabadi, M.R. Saffarian, R. Pourrajab, M. Ghalambaz, Entropy analysis for nanofluid flow over a stretching sheet in the presence of heat generation/absorption and partial slip, J. Mech. Sci. Technol. 27 (2013) 927–937, https://doi.org/10.1007/s12206-013-0104-0.

[44] S.J. Liao, On the Proposed Homotopy Analysis Techniques for Nonlinear Problems and Its Applications, Shanghai Jiao Tong University, Shanghai, China, 1992 ⟨http://www.scirp.org/(S(351jmbntvnsjt1aadkposzje))/reference/ReferencesPapers.aspx?ReferenceID=907&769⟩.

[45] S.J. Liao, Beyond Perturbation: Introduction to the Homotopy Analysis Method, Chapman & Hall/CRC Press, London/Boca Ratton, 2003 ⟨https://www.crcpress.com/Beyond-Perturbation-Introduction-to-the-Homotopy-Analysis-Method/Liao/p/book/9781584884071⟩ (Accessed 28 June 2017).

[46] A.H. Nayfeh, Perturbation Methods, Wiley, New York, USA, 2000 ⟨http://www.wiley.com/WileyCDA/WileyTitle/productCd-0471399175.html⟩ (Accessed 11 April 2017).

[47] F. Mabood, W.A. Khan, Homotopy analysis method for boundary layer flow and heat transfer over a permeable flat plate in a Darcian porous medium with radiation effects, J. Taiwan Inst. Chem. Eng. 45 (2014) 1217–1224, https://doi.org/10.1016/j.jtice.2014.03.019.

[48] B. Raftari, F. Parvaneh, K. Vajravelu, Homotopy analysis of the magnetohydrodynamic flow and heat transfer of a second grade fluid in a porous channel, Energy 9 (2013) 625–632, https://doi.org/10.1016/j.energy.2013.07.054.

[49] N. Shukla, P. Rana, O.A. Beg, B. Singh, Effect of chemical reaction and viscous dissipation on MHD nanofluid flow over a horizontal cylinder: analytical solution, AIP Conf. Proc. 1802 (2017) 020015 (1-8), https://doi.org/10.1063/1.4973265.

[50] N. Shukla, P. Rana, Unsteady MHD nanofluid flow past a stretching sheet with Stefan blowing effect: HAM solution, AIP Conf. Proc. 1897 (2017) 020037, https://doi.org/10.1063/1.5008716.

[51] K. Zaimi, A. Ishak, I. Pop, Unsteady flow due to a contracting cylinder in a nanofluid using Buongiorno's model, Int. J. Heat Mass Transf. 68 (2014) 509–513, https://doi.org/10.1016/j.ijheatmasstransfer.2013.09.047.

[52] R.A. Van Gorder, K. Vajravelu, On the selection of auxiliary functions, operators, and convergence control parameters in the application of the homotopy analysis method to nonlinear differential equations: a general approach, Commun. Nonlinear Sci. Numer. Simul. 14 (2009) 4078–4089, https://doi.org/10.1016/j.cnsns.2009.03.008.